Method of characteristics to evaluate steady 2D flow in a supersonic nozzle

Harsharaj Parmar, Purdue University, West Lafayette, IN, 47907
Submitted as a project report for ME510 Gas Dynamics

1 Model description

The flowchart shown on the next page gives a brief overview of the algorithm used to find the parameters involved in the method of characteristics. A detailed explanation of how the parameters are calculated and the inverse Prandtl-Meyer function is now provided for closure.

Before beginning, a crucial nomenclature used in the flowchart that is *fronts* is explained using Fig.1. Fronts in the current study depict the group of points like [1,2,3,4,5,6,7], [9,10,11,12,13,14] in Fig. 1 and so on. Thus, if we have n expansion waves in our computation then we have n fronts in our plane with the first front being the group [1,2...,n] and progressed to the right.

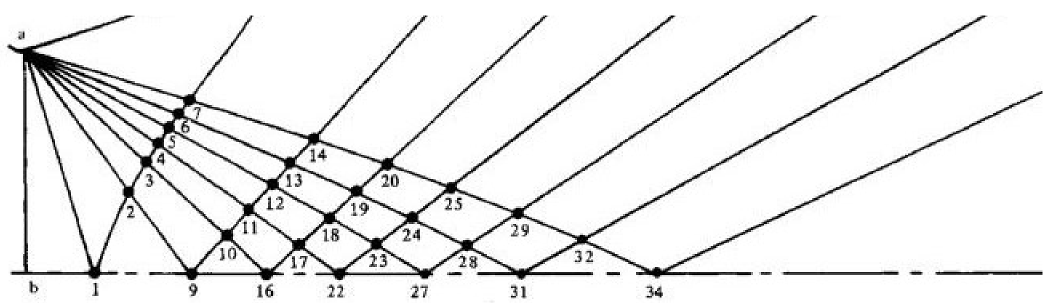

Figure 1: Illustrative plot of characteristics [*Anderson*].

1.1 Initialization

- Using M_{exit} find θ_{max}. Consider Fig. 1 where we see that point 34 has no expansion wave interactions downstream of it so M_{exit} has been achieved there. Also a C_- characteristic runs from point a to 34 which implies that,

$$K_-(a) = K_-(34) \qquad \Longrightarrow \qquad \theta_{max} + \nu_a = \theta_{34} + \nu_{34}$$

Since 34 lies on centerline ($\theta_{34} = 0$) and expansion at a is from sonic conditions ($\Delta\theta = \nu_a$) we get,

$$2\theta_{max} = \nu_e \qquad \Longrightarrow \qquad \theta_{max} = \frac{\nu_e}{2}$$

where ν_e is obtained from M_{exit} and Prandtl-Meyer relation.

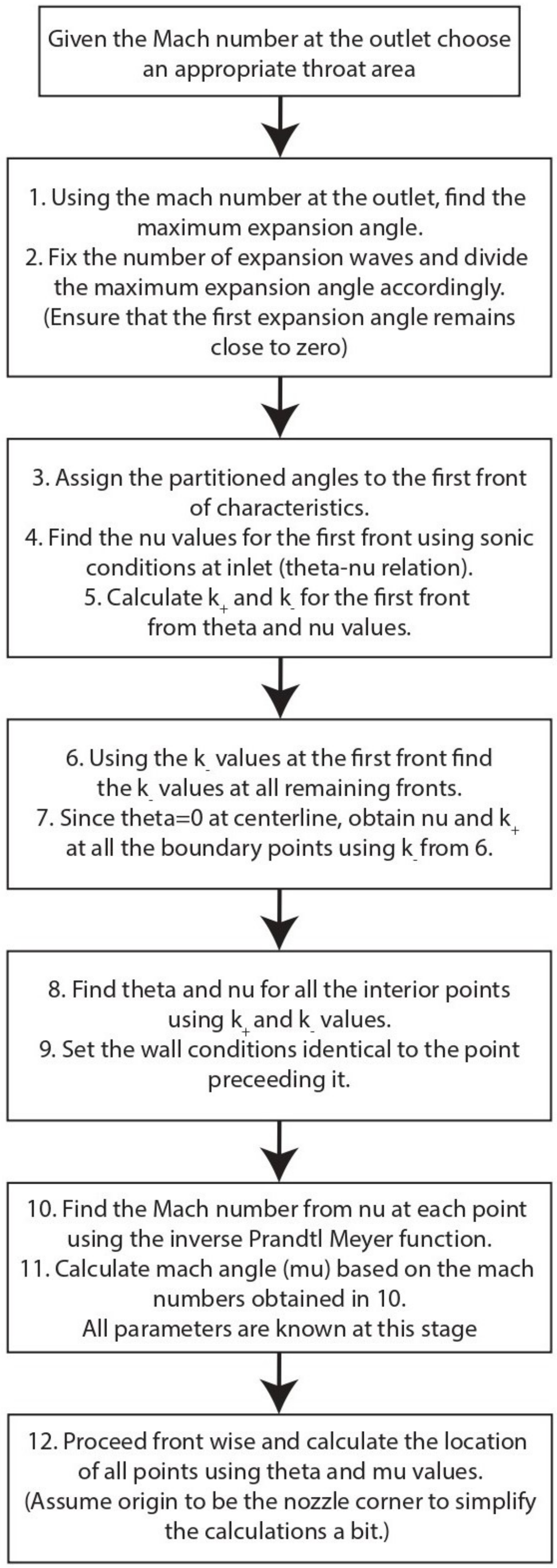

Figure 13: Flowchart depicting the computational steps

- Based on the number of expansion waves n we partition θ_{max} and calculate the total number of points n_{total} from,

$$n_{total} = \frac{(n+1)(n+2)}{2} - 1$$

1.2 First front and boundary evaluations

- In the first front we know that the expansion has taken place from sonic inlet and so from $\theta - \nu$ relation we have $\theta_i = \nu_i$. This implies that for the first front both θ and ν values are known and we can find the K_+ and K_- values using,

$$K_+ = \theta - \nu \qquad K_- = \theta + \nu$$

- Notice that all the C_- characteristics originate from nozzle corner "a" so is we know the K_- values at the first front then we can propagate them downstream. This downstream sweep assigns K_- values to all the points in the domain.

- Now at the centerline boundary we have $\theta = 0$ and using the K_- values obtained before we can find the other parameters,

$$\nu = K_- \qquad K_+ = -K_-$$

  At this point we know the centerline boundary parameters and the first front parameters. Also, note that nozzle wall has the same properties as the point preceding it on the front so the wall values will be updated at the end once all the interior values have been evaluated.

1.3 Interior evaluations

- Moving to interior points we note that all the C_+ characteristics arise from the centerline boundary points and since we have already evaluated the K_+ values at these boundary points we can use them for K_+ values at all the interior points.

- Considering the second front in Fig. 1 for instance, we know the K_+ at 9 (since its a boundary point) and hence we can propagate it along the front to [10,11,12,13,14]. Now both K_- and K_+ values are known for interior points of the second front and we can find θ and ν from,

$$\theta = \frac{(K_- + K_+)}{2} \qquad \nu = \frac{(K_- - K_+)}{2}$$

  This procedure is carried out for all the fronts and so we get properties at all the interior points.

1.4 Nozzle wall evaluations

- Properties at the nozzle wall are identical to those at points before it on the fronts because no expansion wave interaction occurs between them. Since all interior points have been evaluated the nozzle wall calculations are relatively easy and straightforward.

1.5 Inverse Prandtl-Meyer function and Mach angle

- At this point we have the values of θ and ν at all the points in the domains and we move on to finding the Mach number. For a given Mach number we have a relation to obtain ν but the inverse relation cannot be solved for analytically. Many studies use polynomial data-fitted relations to find M corresponding to a particular ν. Here the polynomial is adopted from "Inversion of Prandtl-Meyer Relation",Hall, 1975 given as,

$$M = \frac{1 + Ay + By^2 + Cy^3}{1 + Dy + Ey^2}$$

where $y = \left(\frac{\nu}{\nu_\infty}\right)^{2/3}$ and $\nu_\infty = \frac{\pi}{2}\left(\sqrt{6} - 1\right)$ with the constants given for $\gamma = 1.4$ as,

A	1.3604
B	0.0962
C	-0.5127
D	-0.6722
E	-0.3278

The accuracy of approximation used is quite good with maximum error less than 0.01% in the range of ν $(0 - 50°)$ presented by the current problem as shown in Fig. 2.

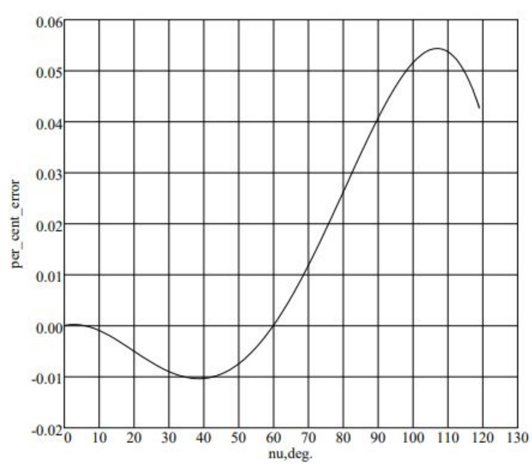

Figure 2: Error plot for Hall approximation with ν [*I. M. Hall, 1975*]

- Once the Mach number is obtained at each point in the domain then the Mach angle can be calculated at each point by using,

$$\mu = \sin^{-1}\left(\frac{1}{M}\right)$$

All property evaluations have been completed at this stage and the only step remaining is to define the location of points in the domain.

1.6 Locating points in the domain

- For simplicity we set the origin to be the nozzle corner point "a" in Fig. 1 from which expansion waves emanate and the throat half length to be 1 unit. The throat half length gives us the y coordinates for all the centerline boundary points given the origin at a.

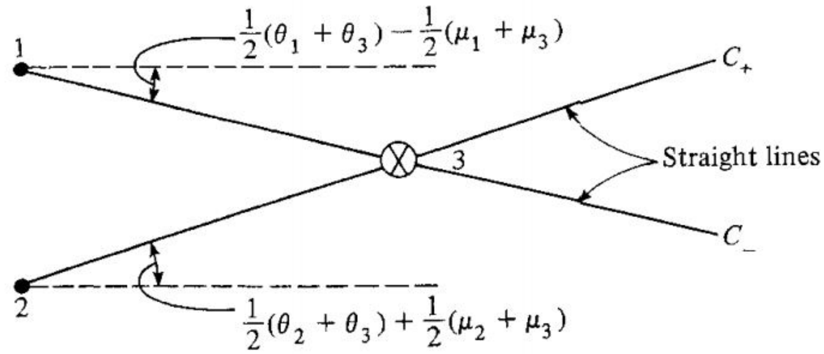

Figure 3: Schematic showing slopes of characteristic lines [*Anderson*]

- Using the slope relations given in Fig. 3 for C_- and C_+ characteristics we can find the location of point 3 given the coordinates of 1 and 2 (note that the points in Fig. 3 do not represent the actual case but are solely for representation).

- The angles for nozzle wall points are a little different from those in the interior, precisely the C_- characteristic slope differs and is given by,

$$tan(\theta_{C_-,i}) = \frac{\theta_i + \theta_{max}}{2} \quad for \quad i = 1 \qquad tan(\theta_{C_-,i}) = \frac{\theta_i + \theta_{i-1}}{2} \quad for \quad i \geqslant 2$$

where i represents the front under consideration and $i-1$ the previous front.

- Referring to Fig. 1, we first determine location of 1 using C_- slope and the throat half length. From there we proceed up the first front and determine the locations using $(0,0)$, previously calculated coordinates and slopes given in Fig. 3.

- Once all points on a front are calculated we move to the next front and march from the boundary point up towards the nozzle wall. Finally, we get the coordinates for all points in the domain and post process the data to visualize the expansion waves and nozzle surface design.

2 Turning angle at Mach 3.0

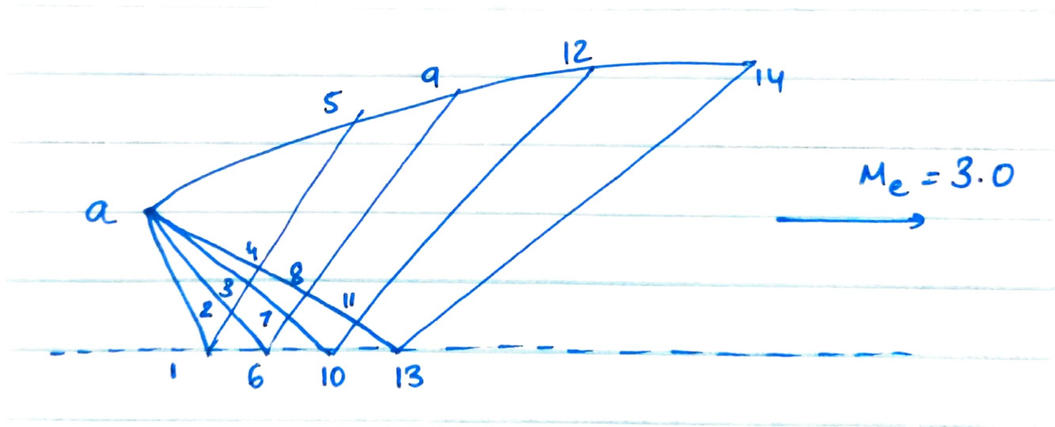

Figure 4: Rough schematic of nozzle with four expansion waves

Let us consider the rough schematic in Fig. 4 to understand the calculation of maximum turning angle at the corner. In particular focusing on points 14, 13 and a we see that point 14 is at the exit condition and since there are no expansion waves between 13 and 14, the same exit conditions persist at 13.

$$\nu_{14} = \nu_{13} = \nu(3.0)$$

Moreover, point 13 lies on the centerline and so,

$$\theta_{13} = 0 \qquad \Longrightarrow \qquad K_{-,13} = \theta_{13} + \nu_{13} = \nu(3.0)$$

Now a C_- characteristic runs from a to 13 ($a - 4 - 8 - 11 - 13$) and along a C_- characteristic the value of K_- remains constant.

$$K_{-,a} = K_{-,13} \qquad \Longrightarrow \qquad \theta_a + \nu_a = \nu(3.0)$$

The maximum turning at a results in $\theta_a = \theta_{max}$ and since the expansion at a is a Prandtl-Meyer expansion from initially sonic conditions we have $\nu_a = \theta_{max}$ which gives us,

$$\theta_{max} = \frac{\nu(3.0)}{2}$$

Using the Prandtl-Meyer function with $\gamma = 1.4$ or Table A.5 from Anderson we get,

$$\nu(3.0) = 49.7574° \qquad \Longrightarrow \qquad \theta_{max} = 24.8787°$$

We get the maximum turning angle to be $\theta_{max} = 24.8787°$ and this would be partitioned to obtain the θ for each expansion wave. In most computations the θ for first expansion wave (a-1 in Fig. 4) is ensured to be as close to 0 as possible. This is because 1 lies on the centerline and so by default has $\theta = 0$ but we supply a non-zero value and this causes an inconsistency. In this study θ_1 is set to 0.2787° and the rest of 24.6° are partitioned as needed.

3 Results

Computational results are obtained for the nozzle with four, five, seven and nine expansion waves. As mentioned before in each computation θ_1 is set to a small value of 0.2787° to avoid any inconsistencies and the rest of 24.6° are divided as per requirement. Some notable observations can be listed as follows,

- Increasing the number of expansion waves results in better resolution of the flow since more characteristics now span θ_{max} giving a closely spaced net across the nozzle.
- Good correspondence is obtained with quasi-1D flow area ratio at the outlet even when only four expansion waves are used.

As a consequence of these observations the nozzle geometry, wave patterns, centerline and wall Mach number results are all plotted for the case of nine expansion waves where the flow is best resolved.

3.1 Characteristic lines and geometry

The coordinates mentioned in the plot given in Fig. 5 describe the last point in the domain and help in determining the nozzle length and numerical area ratio at the outlet of the nozzle.

$$l_{min} = x_e = 16.9309$$

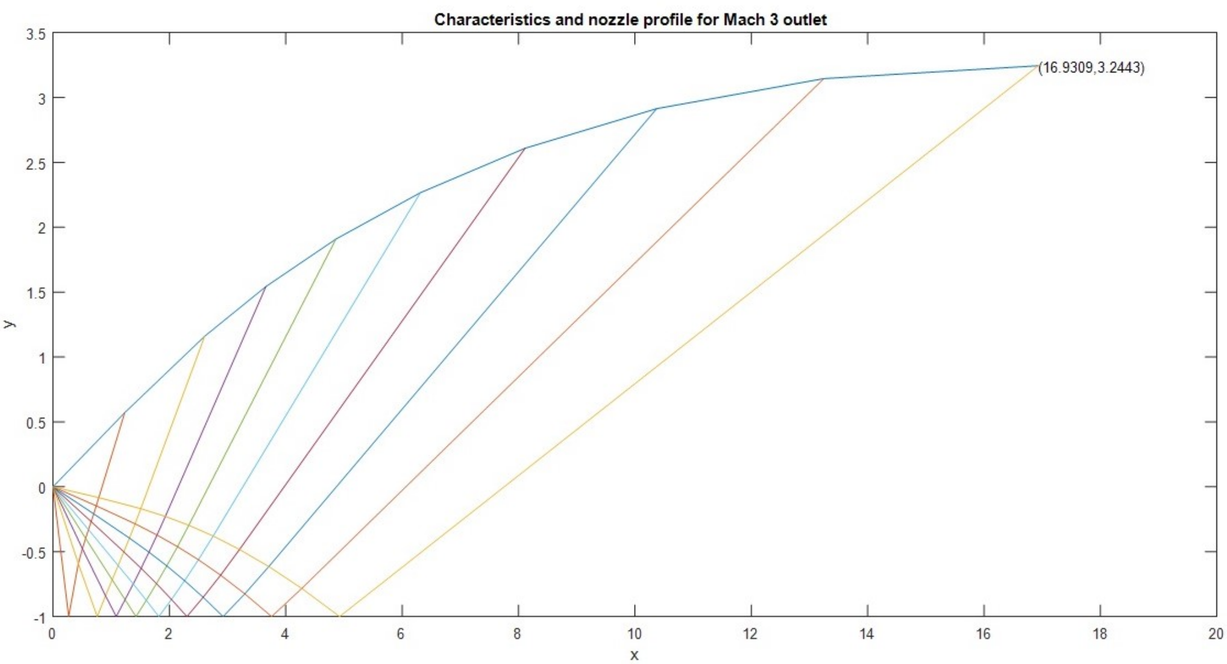

Figure 5: Characteristic lines and nozzle surface profile for nine expansion waves

3.2 Mach numbers at wall and centerline

Mach number are plotted along nozzle length at the wall and centerline with M set to 1 at $x = 0$ as shown in Fig. 6. Notice that at the centerline we only have points till $x = 5$ and so the plot terminates earlier than the wall case where the entire length is covered.

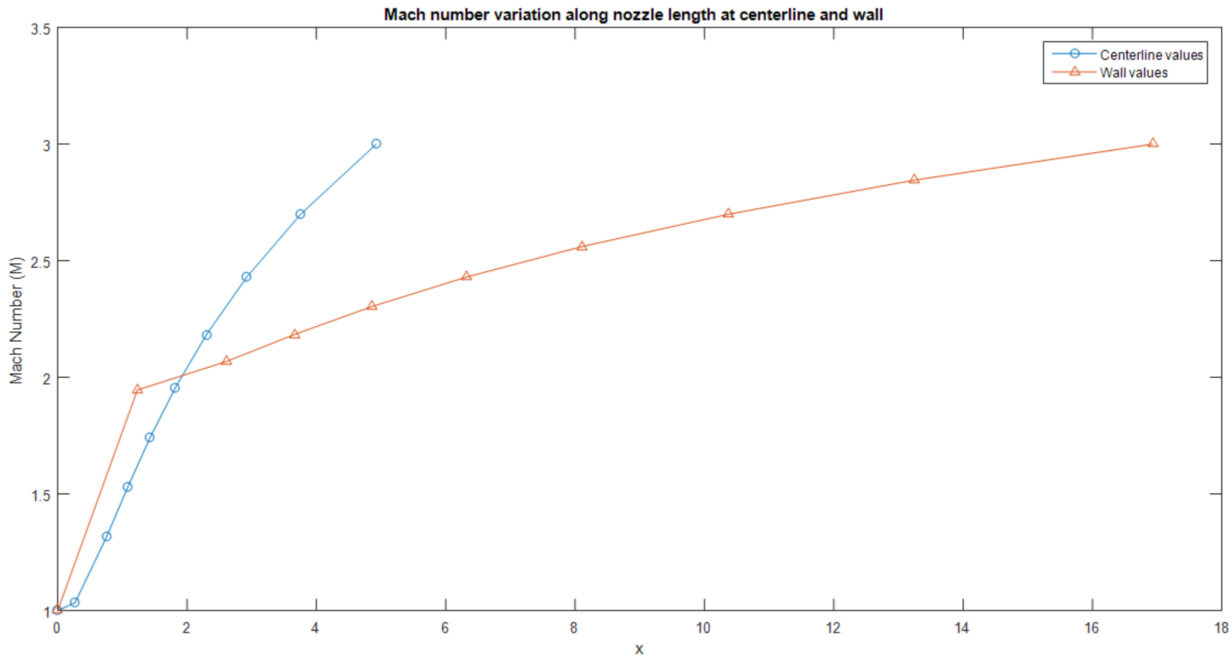

Figure 6: Plot of centerline and wall mach numbers along the length of the nozzle for nine expansion waves

3.3 Convergence analysis

Convergence in the solution can be examined from the plots given in Fig. 7 and 8 by checking their separation. Firstly, the results in both plots are very close to each other which suggests that the method works well even at lower number of expansion waves. Secondly, looking into Fig. 7 for centerline mach numbers we observe visible dispersion in Mach number values from $x = 3 - 4$. The lowest line in purple represents 4 expansion waves and differs considerably from values at 7 and 9 expansion waves case which are very close.This shows that as we increase the number of waves the plots move closer to each other to represent a singular solution which is the essence of convergence.

Similarly, considering the plot in Fig. 8 we note a considerable variance from $x = 10 - 14$ and the case of 4 expansion waves slightly under predicts the Mach number. Here again the results for 7 and 9 expansion waves are very close to each other and represent the notion that as we increase the number of waves we would get a converged solution. The spreading decreases as we move to higher number of expansion waves (4-5-7-9) and thus denotes convergence.

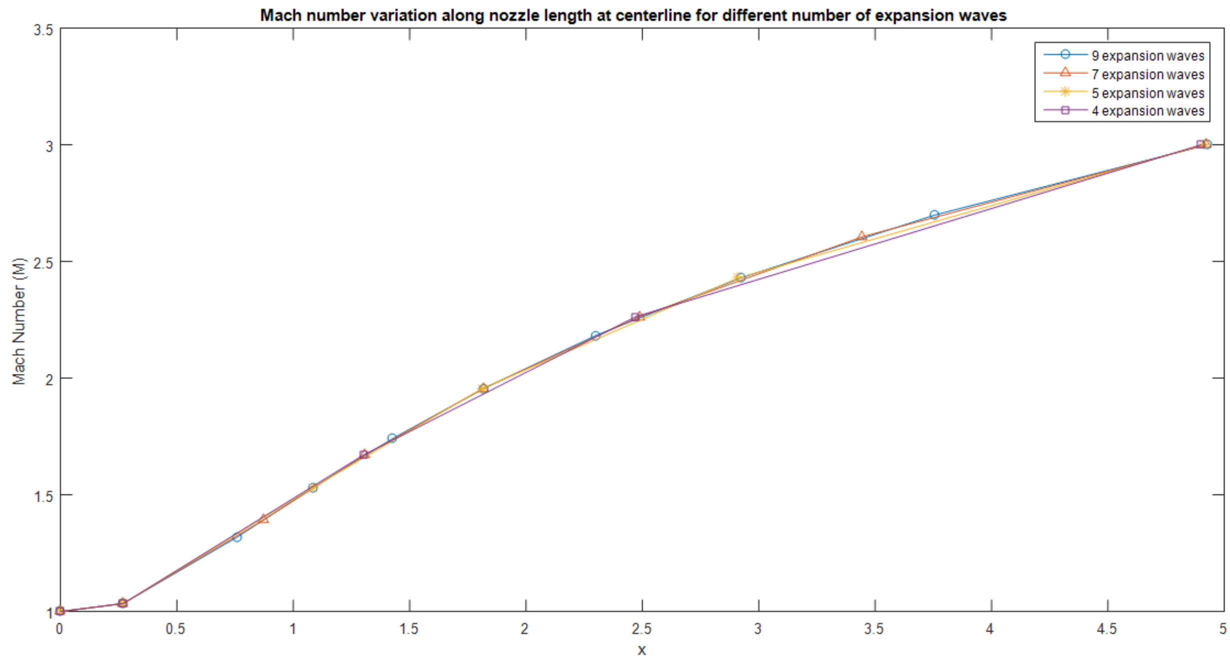

Figure 7: Plot of centerline mach numbers along the length for different number of expansion waves.

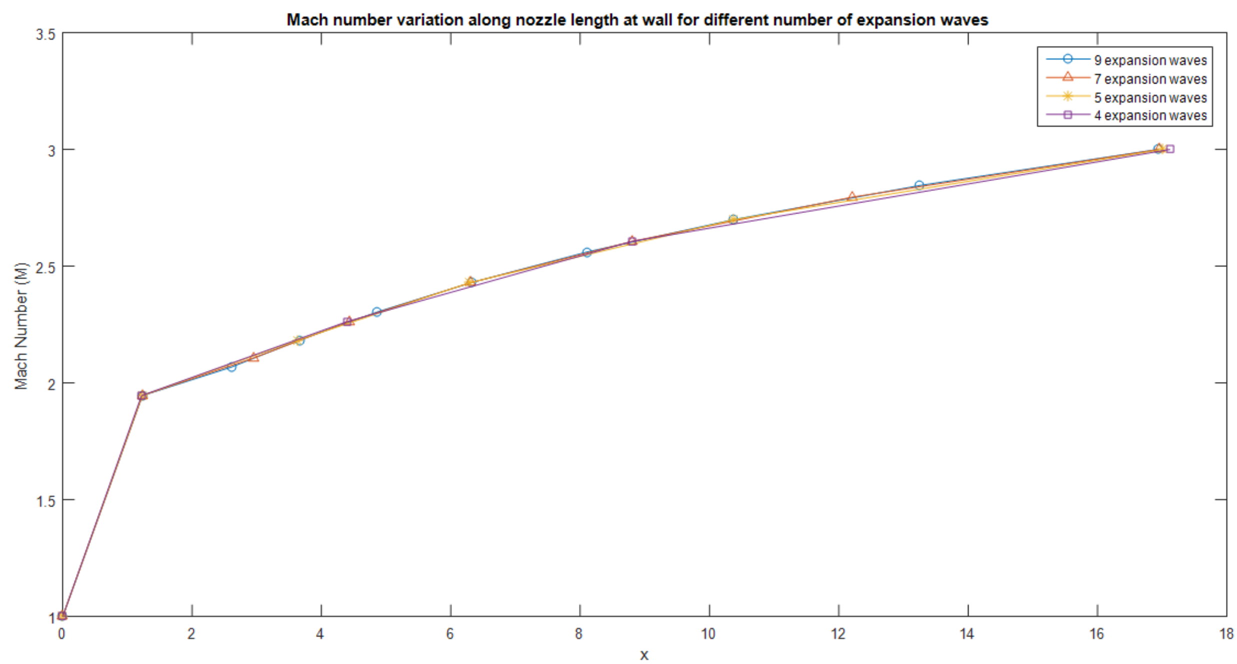

Figure 8: Plot of centerline mach numbers along the length for different number of expansion waves.

3.4 Minimum nozzle length

The term *minimum* nozzle length is used because the nozzle design adopted here excludes the expansion section which gradually changes the turning angle to θ_{max} from the throat.

If the expansion section is included then the length of the nozzle increases attributed to the gradual change in turning angle. In our computations the maximum turning angle is applied straight away and so the length of nozzle is said to be minimum. As seen from the convergence studies, solution obtained at 9 expansion waves is the most accurate and is very close to the converged solution. Reverting back to Fig. 5 we observe that the coordinates of last point in the domain are (16.9309,3.2443) which implies that,

$$l_{min} = 16.9309$$

where the unit can be defined based on given units of throat area. Here $l_{min} = 16.9309$ units since half throat length is taken to be 1 unit. Also as seen in Fig. 9, 10 and 11 the nozzle length increases with decrease in the number or expansion waves and so 9 expansion waves indeed gives us the minimum calculated nozzle length.

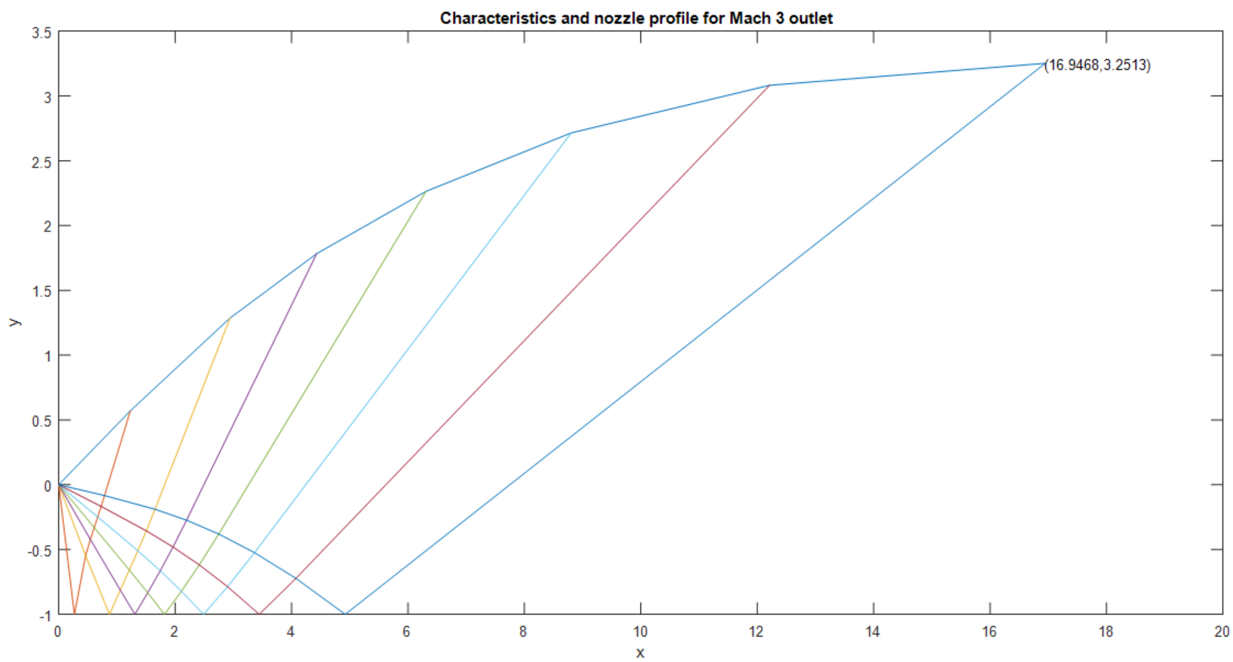

Figure 9: Characteristic lines and nozzle surface profile for seven expansion waves.

3.5 Quasi 1-D flow comparison

In this section a comparison is laid out between the numerical results obtained from solution of nine expansion waves in the nozzle and quasi 1-D flow results. Two comparisons are shown one graphical and the other quantitative. Graphical comparison is drawn using the numerical area ratio prevalent at the wall points and the computed area ratio from quasi 1-D flow relation at given wall Mach numbers.

3.5.1 Graphical area ratio comparison along nozzle length

Wall Mach number variation with length was considered in Fig. 8 but here we shall observe the computed area ratio and the area ratio from quasi 1-D relations using Mach numbers at

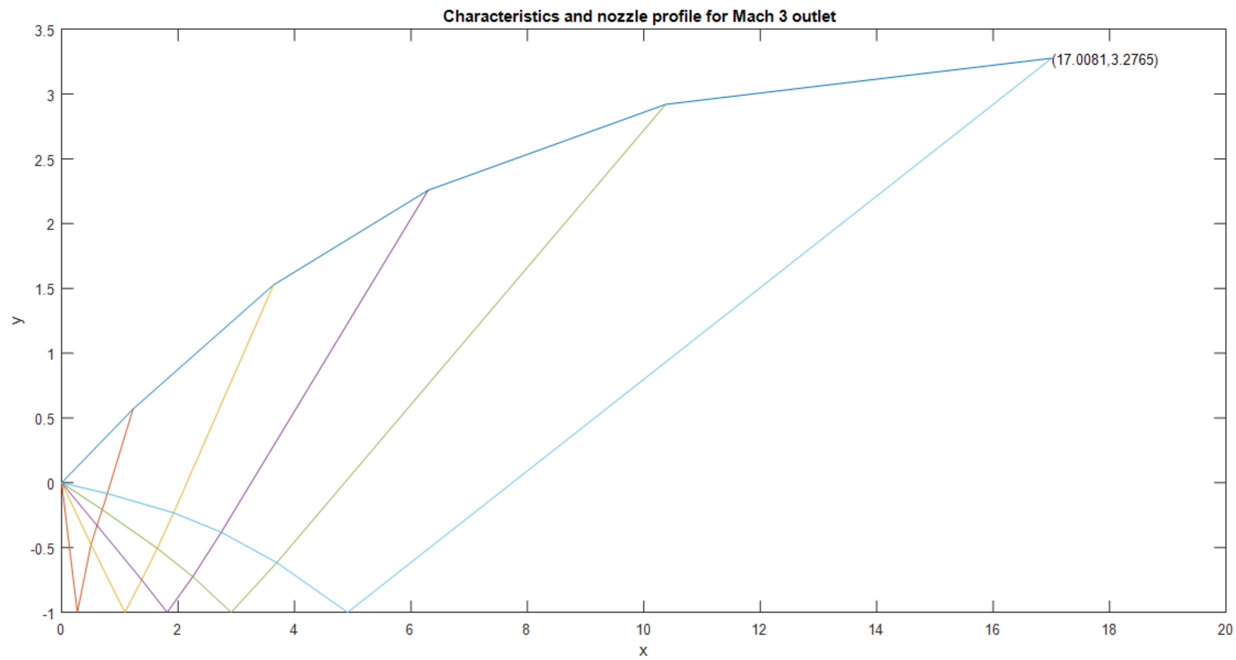

Figure 10: Characteristic lines and nozzle surface profile for five expansion waves.

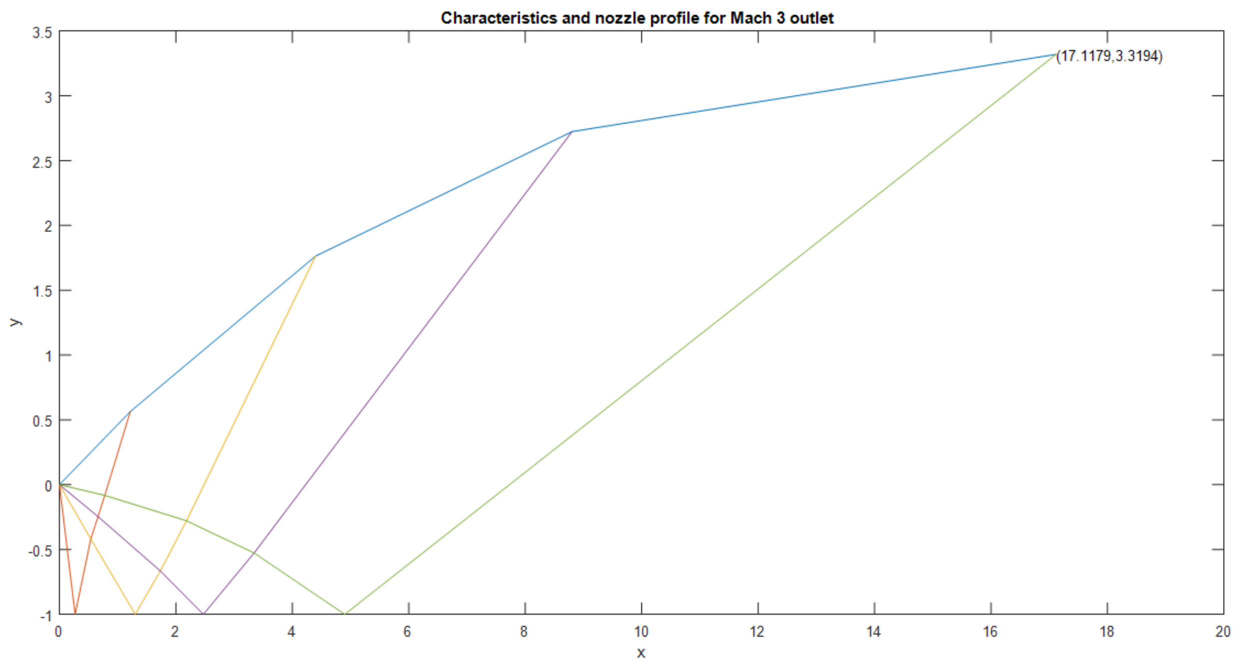

Figure 11: Characteristic lines and nozzle surface profile for four expansion waves.

the wall points along nozzle length. Now for the computed area ratio we have the coordinates of all the wall points and can easily calculate the ratio using,

$$\left(\frac{A}{A^*}\right)_{num,i} = 1 + y_i$$

For the quasi 1-D flow area ratio we use the Mach number at the wall points and plot them with length along with the numerical ratios.

$$\left(\frac{A}{A^*}\right)^2_{1D,i} = \frac{1}{M_i^2}\left[\frac{2}{\gamma+1}\left(1+\frac{\gamma-1}{2}M_i^2\right)\right]^{(\gamma+1)/(\gamma-1)}$$

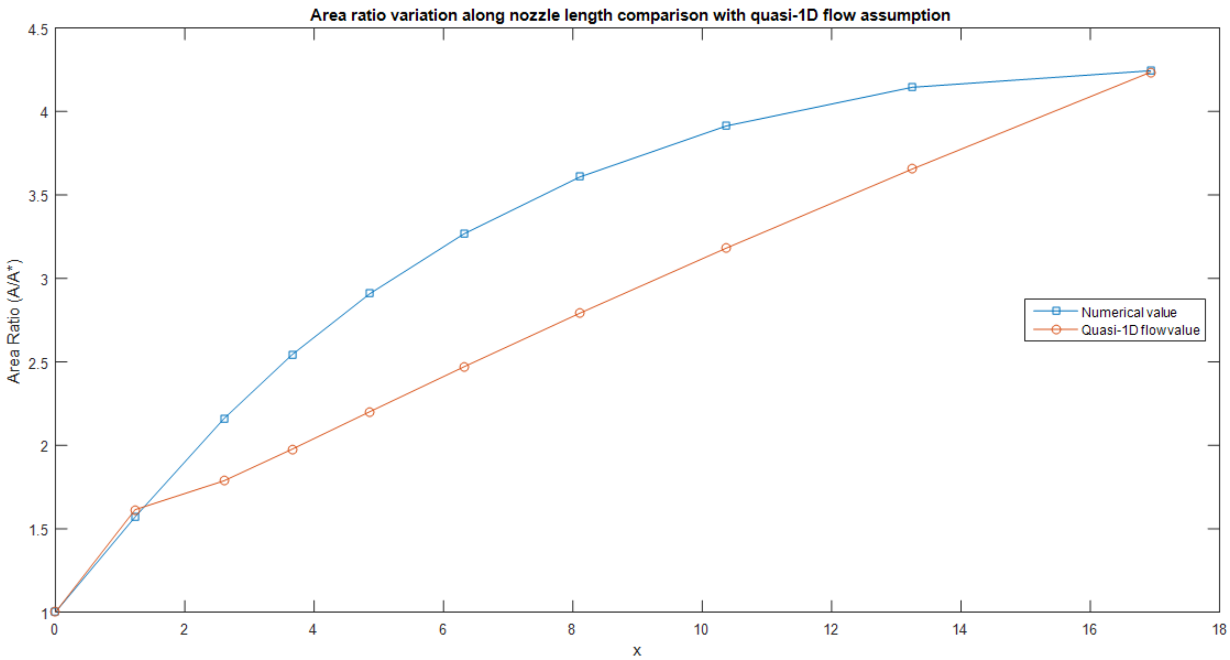

Figure 12: Area ratio comparison of numerical results with quasi 1-D flow results for the case of nine expansion waves.

Interesting observations can be made from the plot shown in Fig 12.

1. For the same Mach number and throat area, computed nozzle area is greater than the quasi 1-D flow area. Assuming equal stagnation temperatures, we have equal temperature and subsequently equal flow velocities along the length of the nozzle for both cases.

2. Moreover, the throat is choked in both the cases so mass flow rate is fixed and equal. Now for equal flow velocity and mass flow rate, since computed area is greater the density prevalent should be lower than the quasi 1-D flow case.

3. Lower density in the computations indicates lower pressures from ideal gas law and so we have that pressures are lower inside the nozzle in the computations than quasi 1-D results. Expansion is greater in computations than 1-D case.

4. This is in accordance to our expectations because expansion wave interactions result in pressure drops in our computations and those are absent in 1-D analysis. Note that expansion waves begin interacting at the wall after the first wall point and so deviations are observed after the same.

5. Finally as we move to end of the nozzle the expansion interactions reduce to the extent that at the last wall point no expansion waves exist which has been seen earlier in the report. As a result of this, the curves move closer to each other and converge at the end to result in the same area ratio and pressure drop across the nozzle.

3.5.2 Outlet area ratio comparison

For the given $M_e = 3.0$ we can get the area ratio at outlet from quasi 1-D flow analysis and compare it with the numerical ratio. Using compressible flow calculator at $M = 3.0$ we have,

$$\left(\frac{A}{A^*}\right)_{1D} = 4.2346$$

From Fig. 5, 9, 10, 11 and $\left(\frac{A}{A^*}\right)_{num,e} = 1 + y_e$ we get the following values,

Table 1: Outlet area ratio comparison

Number of expansions	$\left(\frac{A}{A^*}\right)_e$	%error
9	4.2443	0.2291
7	4.2513	0.3944
5	4.2765	0.9895
4	4.3194	2.0026

Table 1 clearly shows that the numerical model gives decent results for four expansion waves and high fidelity solutions for seven and nine expansion wave cases (error drops below 0.5%).

4 Conclusion

In conclusion we can say that method of characteristics can accurately resolve steady two dimensional flow problems in nozzle design and achieve high levels of accuracy. For the current problem with $M_e = 3.0$ we get the minimum nozzle length $l_{min} = 16.9309$ with nine expansion waves spanning the maximum turning angle. Area ratio at the exit is found to be $\left(\frac{A}{A^*}\right)_e = 4.2443$ and exhibits an error of 0.2291% compared to quasi one dimensional flow solution.

Convergence studies have been done from Mach number plots at wall and centerline and can be assumed to be established after seven expansion waves for this problem. The solution with nine expansion waves is the closest to the converged solution and can be deemed useful for design.